JOURNAL OF COMPUTATIONAL PHYSICS 100, 355–363 (1992)

Multi-domain Chebyshev–Fourier Method for the Solution of the Equations of Motion of Dynamic Elasticity

EKKEHART TESSMER

Institut für Geophysik, Universität Hamburg, D 2000 Hamburg, Germany

DAVID KESSLER

Department of Geophysics and Planetary Sciences, Tel Aviv University, Tel Aviv, Israel 69978

DAN KOSLOFF

Institut für Geophysik, Universität Hamburg, D 2000 Hamburg, Germany, and Department of Geophysics and Planetary Sciences, Tel Aviv University, Tel Aviv, Israel 69978

AND

ALFRED BEHLE

Institut für Geophysik, Universität Hamburg, D 2000 Hamburg, Germany

Received October 30, 1990; revised August 8, 1991

A multi-domain approach for the solution of the equations of elasticity in two spatial dimensions is presented. The equations of momentum conservation and the stress–strain relations are recast as a system of five coupled equations in time in which the particle velocities and the stresses are the unknowns. Solution schemes for both 2D Cartesian and polar coordinates are derived. In both cases the solution is assumed periodic in one coordinate (the x or θ directions) and non-periodic in the other direction. The numerical algorithm uses a Fourier expansion in the periodic direction and domain decomposition and a modified Chebyshev expansion in the remaining direction. The multi-domain approach is tested against problems with known solutions. In all cases it appears as accurate as solutions with a single domain. The multi-domain concept adds flexibility and improves efficiency. It allows use of different grid sizes in different regions depending on the material properties and allows a relatively uniform grid spacing in the polar coordinate case.

INTRODUCTION

We introduce a multi-domain spectral method for the solution of the equations of dynamic elasticity. Multi-domain approaches for solving partial differential equations have found wide use in computational physics in situations where a single global expansion is no longer adequate ([1], for a review). In the problems tackled in this study, the reasons for the multi-domain approach have either been a change in the governing equations in the domains when fluid regions and solid regions are in juxtaposition, or geometrical considerations.

This work involves elastic wave propagation in two spatial dimensions in the context of exploration geophysics. We first examine solutions in Cartesian coordinates where one coordinate points in the vertical direction and the other in the horizontal direction. Due to this configuration we used a Fourier expansion for the horizontal direction and a modified Chebyshev expansion for the vertical direction [2, 3]. The domain decomposition is performed in the vertical direction into horizontal strips (Fig. 1).

The second application studied is for the solution in 2D circular coordinates. In this case the angular θ coordinate is naturally periodic and hence a Fourier expansion was used fo that direction. For the radial direction we again used a modified Chebyshev expansion. The domain decomposition is for the radial direction in the form of rings. Each ring contains more grid points in the θ direction than the ring preceding it. This enables a relatively uniform spatial sampling and hence circumvents the disadvantage of circular grids to radially expand in the θ direction. The stability of the numerical algorithm is improved by orders of magnitude over the single grid case.

The matching of solutions between domains is based on requiring continuity of tractions and displacements and

0021-9991/92 $5.00

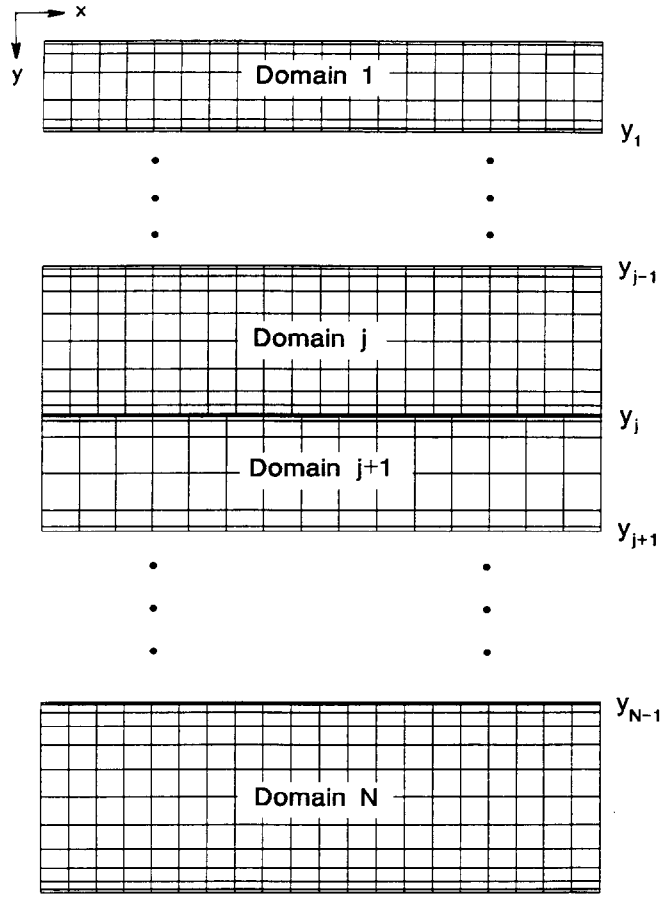

FIG. 1. Decomposition of a medium into different domains.

that outward moving variables on the boundary remain unchanged. This is equivalent to the upwind condition in [1]. In the following sections we first present the equations of motion in Cartesian coordinates and describe the solution algorithm and domain decomposition. Next, the equations in circular coordinates are derived. We then present a number of examples which test the accuracy of the multi-domain approach.

EQUATION OF MOTION IN CARTESIAN COORDINATES

Let x and y respectively denote the horizontal and vertical Cartesian coordinates. For an isotropic elastic solid undergoing infinitesimal deformation the equations of motion can be recast as a first-order system given by

$$\frac{\partial}{\partial t}\begin{pmatrix}\dot{u}_x\\ \dot{u}_y\\ \sigma_{xx}\\ \sigma_{yy}\\ \sigma_{xy}\end{pmatrix}=\mathbf{A}\begin{pmatrix}\dot{u}_x\\ \dot{u}_y\\ \sigma_{xx}\\ \sigma_{yy}\\ \sigma_{xy}\end{pmatrix}_x+\mathbf{B}\begin{pmatrix}\dot{u}_x\\ \dot{u}_y\\ \sigma_{xx}\\ \sigma_{yy}\\ \sigma_{xy}\end{pmatrix}_y+\begin{pmatrix}f_x/\rho\\ f_y/\rho\\ 0\\ 0\\ 0\end{pmatrix}, \tag{1}$$

where

$$\mathbf{A}=\begin{pmatrix}0 & 0 & \rho^{-1} & 0 & 0\\ 0 & 0 & 0 & 0 & \rho^{-1}\\ \lambda+2\mu & 0 & 0 & 0 & 0\\ \lambda & 0 & 0 & 0 & 0\\ 0 & \mu & 0 & 0 & 0\end{pmatrix} \tag{2}$$

and

$$\mathbf{B}=\begin{pmatrix}0 & 0 & 0 & 0 & \rho^{-1}\\ 0 & 0 & 0 & \rho^{-1} & 0\\ 0 & \lambda & 0 & 0 & 0\\ 0 & \lambda+2\mu & 0 & 0 & 0\\ \mu & 0 & 0 & 0 & 0\end{pmatrix}. \tag{3}$$

$\dot{u}_x$ and $\dot{u}_y$ denote the horizontal and vertical particle velocities respectively, σ_{xx}, σ_{yy}, and σ_{xy} are the stress components, ρ is the density, λ and μ are the rigidity and shear modulus, and f_x and f_y are the body forces per unit volume. The system (1) has previously been used by [4–6] for finite difference calculations and by [2] for a Fourier–Chebyshev method.

Equation (1) needs to be supplied with appropriate boundary conditions. For $y=0$ we use a free surface condition which reads

$$\sigma_{xy}=0.$$

$$\sigma_{yy}=0.$$

For the bottom of the grid $y=L$ we apply an absorbing boundary condition to be discussed later. For the horizontal direction we assume periodic boundary conditions. In regions containing fluids the shear stresses σ_{xy} are zero and $\sigma_{xx}=\sigma_{yy}=-p$ with p the pressure. The equations of motion then become

$$\frac{\partial}{\partial t}\begin{pmatrix}\dot{u}_x\\ \dot{u}_y\\ -p\end{pmatrix}=\mathbf{A}\begin{pmatrix}\dot{u}_x\\ \dot{u}_y\\ -p\end{pmatrix}_x+\mathbf{B}\begin{pmatrix}\dot{u}_x\\ \dot{u}_y\\ -p\end{pmatrix}_y+\begin{pmatrix}f_x/\rho\\ f_y/\rho\\ 0\end{pmatrix}, \tag{4}$$

where

$$\mathbf{A}=\begin{pmatrix}0 & 0 & \rho^{-1}\\ 0 & 0 & 0\\ K & 0 & 0\end{pmatrix} \tag{5}$$

and

$$\mathbf{B}=\begin{pmatrix}0 & 0 & 0\\ 0 & 0 & \rho^{-1}\\ 0 & K & 0\end{pmatrix}, \tag{6}$$

with K the bulk modulus. The free surface condition for the fluid is $p=0$.

The application of boundary conditions at $y=0$ and $y=L$ and the requirement of continuity at subdomain boundaries is based on allowing only inward moving characteristic variables to be modified [7]. Based on a one-dimensional analysis in which only vertical derivatives are considered, Eq. (1) has the five characteristic variables $\dot{u}_x \pm (1/\rho v_s)\,\sigma_{xy}$, $\dot{u}_y \pm (1/\rho v_p)\,\sigma_{yy}$ and $\sigma_{xx} - (\lambda/(\lambda+2\mu))\,\sigma_{yy}$ [6, 3], where $v_p = \sqrt{(\lambda+2\mu)/\rho}$ and $v_s = \sqrt{\mu/\rho}$ are respectively the P wave and S wave velocities. These characteristics respectively move with the velocities $\pm v_s$, $\pm v_p$, and zero. For fluid regions, Eq. (4) has the three characteristic variables, $\dot{u}_y \mp p/\rho v_p$ which move with velocities $\pm v_p$ with $v_p = \sqrt{K/\rho}$ and the zero characteristic $\dot{u}_x$.

Application of Boundary Conditions and Domain Decomposition

In a typical calculation the operator on the right-hand side of Eq. (1) acts on a vector of variables $(\dot{u}_x, \dot{u}_y, \sigma_{xx}, \sigma_{yy}, \sigma_{xy})^{\mathrm{T}}$ to yield an output vector which we denote as $(\dot{u}_x^{\mathrm{old}}, \dot{u}_y^{\mathrm{old}}, \sigma_{xx}^{\mathrm{old}}, \sigma_{yy}^{\mathrm{old}}, \sigma_{xy}^{\mathrm{old}})^{\mathrm{T}}$. This vector is then updated to satisfy an appropriate boundary condition or continuity condition as well as the requirement that the outward moving characteristics remain unmodified [7]. The resulting vector is denoted by $(\dot{u}_x^{\mathrm{new}}, \dot{u}_y^{\mathrm{new}}, \sigma_{xx}^{\mathrm{new}}, \sigma_{yy}^{\mathrm{new}}, \sigma_{xy}^{\mathrm{new}})^{\mathrm{T}}$. For the traction free boundary condition $\sigma_{xy}=\sigma_{yy}=0$ at $y=0$ the modification procedure implies [2],

$$\begin{aligned}
\dot{u}_x^{\mathrm{new}} &= \dot{u}_x^{\mathrm{old}} + \frac{1}{\rho v_s}\,\sigma_{xy}^{\mathrm{old}} \\
\dot{u}_y^{\mathrm{new}} &= \dot{u}_y^{\mathrm{old}} + \frac{1}{\rho v_p}\,\sigma_{yy}^{\mathrm{old}} \\
\sigma_{xx}^{\mathrm{new}} &= \sigma_{xx}^{\mathrm{old}} - \frac{\lambda}{\lambda+2\mu}\,\sigma_{yy}^{\mathrm{old}}.
\end{aligned} \tag{7}$$

For the boundary $y=L$ we used the absorbing condition that the inward characteristic is zero [6, 2]. This gives

$$\begin{aligned}
\sigma_{xy}^{\mathrm{new}} &= \tfrac{1}{2}(\sigma_{xy}^{\mathrm{old}} - \rho v_s \dot{u}_x^{\mathrm{old}}) \\
\dot{u}_x^{\mathrm{new}} &= \tfrac{1}{2}(\dot{u}_x^{\mathrm{old}} - \sigma_{xy}^{\mathrm{old}}/\rho v_s) \\
\sigma_{yy}^{\mathrm{new}} &= \tfrac{1}{2}(\sigma_{yy}^{\mathrm{old}} - \rho v_p \dot{u}_y^{\mathrm{old}}) \\
\dot{u}_y^{\mathrm{new}} &= \tfrac{1}{2}(\dot{u}_y^{\mathrm{old}} - \sigma_{yy}^{\mathrm{old}}/\rho v_p) \\
\sigma_{xx}^{\mathrm{new}} &= \frac{\lambda}{\lambda+2\mu}\,(\sigma_{yy}^{\mathrm{new}} - \sigma_{yy}^{\mathrm{old}}).
\end{aligned} \tag{8}$$

In addition to boundary conditions, continuity conditions need to be satisfied upon crossing from one domain to the next. Let y_j denote the vertical coordinate of the bottom of the jth subdomain (Fig. 1). When both the jth subdomain and $(j+1)$th subdomain are composed of solids, the variables $\dot{u}_x$, $\dot{u}_y$, σ_{xy}, and σ_{yy} need to be continuous upon crossing the common interface. The modification procedure at $y=y_j$ then reads

$$\begin{aligned}
\dot{u}_x^{\mathrm{new}} &= \dot{u}_{x(j)}^{\mathrm{new}} = \dot{u}_{x(j+1)}^{\mathrm{new}} \\
&= \frac{1}{2}\left[\dot{u}_{x(j)}^{\mathrm{old}} + \dot{u}_{x(j+1)}^{\mathrm{old}} - \frac{\sigma_{xy(j)}^{\mathrm{old}}}{\rho_{(j)} v_{s(j)}} + \frac{\sigma_{xy(j+1)}^{\mathrm{old}}}{\rho_{(j+1)} v_{s(j+1)}} \right. \\
&\quad \left. + \left(\frac{1}{\rho_{(j)} v_{s(j)}} - \frac{1}{\rho_{(j+1)} v_{s(j+1)}}\right)\sigma_{xy}^{\mathrm{new}}\right]
\end{aligned} \tag{9a}$$

$$\begin{aligned}
\dot{u}_y^{\mathrm{new}} &= \dot{u}_{y(j)}^{\mathrm{new}} = \dot{u}_{y(j+1)}^{\mathrm{new}} \\
&= \frac{1}{2}\left[\dot{u}_{y(j)}^{\mathrm{old}} + \dot{u}_{y(j+1)}^{\mathrm{old}} - \frac{\sigma_{yy(j)}^{\mathrm{old}}}{\rho_{(j)} v_{p(j)}} + \frac{\sigma_{yy(j+1)}^{\mathrm{old}}}{\rho_{(j+1)} v_{p(j+1)}} \right. \\
&\quad \left. + \left(\frac{1}{\rho_{(j)} v_{p(j)}} - \frac{1}{\rho_{(j+1)} v_{p(j+1)}}\right)\sigma_{yy}^{\mathrm{new}}\right]
\end{aligned} \tag{9b}$$

$$\begin{aligned}
\sigma_{xy}^{\mathrm{new}} &= \sigma_{xy(j)}^{\mathrm{new}} = \sigma_{xy(j+1)}^{\mathrm{new}} \\
&= \frac{\rho_{(j)} v_{s(j)} \rho_{(j+1)} v_{s(j+1)}}{\rho_{(j)} v_{s(j)} + \rho_{(j+1)} v_{s(j+1)}} \\
&\quad \times \left(\dot{u}_{x(j+1)}^{\mathrm{old}} - \dot{u}_{x(j)}^{\mathrm{old}} + \frac{\sigma_{xy(j+1)}^{\mathrm{old}}}{\rho_{(j+1)} \dot{u}_{s(j+1)}} + \frac{\sigma_{xy(j)}^{\mathrm{old}}}{\rho_{(j)} v_{s(j)}}\right)
\end{aligned} \tag{9c}$$

$$\begin{aligned}
\sigma_{yy}^{\mathrm{new}} &= \sigma_{yy(j)}^{\mathrm{new}} = \sigma_{yy(j+1)}^{\mathrm{new}} \\
&= \frac{\rho_{(j)} v_{p(j)} \rho_{(j+1)} v_{p(j+1)}}{\rho_{(j)} v_{p(j)} + \rho_{(j+1)} v_{p(j+1)}} \\
&\quad \times \left(\dot{u}_{y(j+1)}^{\mathrm{old}} - \dot{u}_{y(j)}^{\mathrm{old}} + \frac{\sigma_{yy(j+1)}^{\mathrm{old}}}{\rho_{(j+1)} v_{p(j+1)}} + \frac{\sigma_{yy(j)}^{\mathrm{old}}}{\rho_{(j)} v_{p(j)}}\right).
\end{aligned} \tag{9d}$$

In addition the stress component σ_{xx}, which is not necessarily continuous, needs to be updated on both sides of the interface according to

$$\sigma_{xx}^{\mathrm{new}} = \sigma_{xx}^{\mathrm{old}} + \frac{\lambda}{\lambda+2\mu}\,(\sigma_{yy}^{\mathrm{new}} - \sigma_{yy}^{\mathrm{old}}).$$

For a domain containing a fluid the free surface boundary condition $p=0$ implies

$$\dot{u}_y^{\mathrm{new}} = \dot{u}_y^{\mathrm{old}} - \frac{1}{\rho v_p}\,p^{\mathrm{old}}.$$

The continuity requirement between two fluid subdomains is given by (9b) and (9d) with σ_{yy} substituted by $-p$. In this case the horizontal particle velocity $\dot{u}_x$ needs not be continuous. Finally when the jth subdomain is occupied by a fluid and the $(j+1)$th subdomain is occupied by a solid, the condition at the common interface is $\sigma_{xy}=0$, while σ_{yy} (or

$-p$ on the fluid side) and $\dot{u}_y$ remain continuous. This implies

$$\dot{u}^{\text{new}}_{x(j+1)} = \dot{u}^{\text{old}}_{x(j+1)} + \frac{1}{\rho_{(j+1)} v_{s(j+1)}} \sigma^{\text{old}}_{xy(j+1)}$$

$$\sigma^{\text{new}}_{xy(j+1)} = 0$$

$$\dot{u}^{\text{new}}_{y} = \dot{u}^{\text{new}}_{y(j)} = \dot{u}^{\text{new}}_{y(j+1)}$$

$$= \frac{1}{2}\left[\dot{u}^{\text{old}}_{y(j)} + \dot{u}^{\text{old}}_{y(j+1)} + \frac{p^{\text{old}}}{\rho_{(j)} v_{p(j)}} + \frac{\sigma^{\text{old}}_{yy(j+1)}}{\rho_{(j+1)} v_{p(j+1)}} + \left(\frac{1}{\rho_{(j)} v_{p(j)}} - \frac{1}{\rho_{(j+1)} v_{p(j+1)}} \right) \sigma^{\text{new}}_{yy} \right] \tag{10}$$

$$\sigma^{\text{new}}_{yy} = -p^{\text{new}}_{(j)} = \sigma^{\text{new}}_{yy(j+1)}$$

$$= \frac{\rho_{(j)} v_{p(j)} \rho_{(j+1)} v_{p(j+1)}}{\rho_{(j)} v_{p(j)} + \rho_{(j+1)} v_{p(j+1)}} \times \left(\dot{u}^{\text{old}}_{y(j+1)} - \dot{u}^{\text{old}}_{y(j)} + \frac{\sigma^{\text{old}}_{yy(j+1)}}{\rho_{(j+1)} v_{p(j+1)}} - \frac{p^{\text{old}}_{(j)}}{\rho_{(j)} v_{p(j)}} \right)$$

$$\sigma^{\text{new}}_{xx(j+1)} = \sigma^{\text{old}}_{xx(j+1)} + \frac{\lambda_{(j+1)}}{\lambda_{(j+1)} + 2\mu_{(j+1)}} (\sigma^{\text{new}}_{yy(j+1)} - \sigma^{\text{old}}_{yy(j+1)}).$$

The above procedure for the continuity at subdomain boundaries which is based on [7] can be shown to be equivalent to the upwind condition in [1, Eq. (13.2.26), p. 452].

Spatial Discretization and Numerical Solution Method

The numerical algorithm solves Eq. (1) or (4), based on a collocation method in which the solution is expanded by a Fourier expansion in the horizontal direction and a Chebyshev expansion within each subdomain in the vertical direction (Fig. 2).

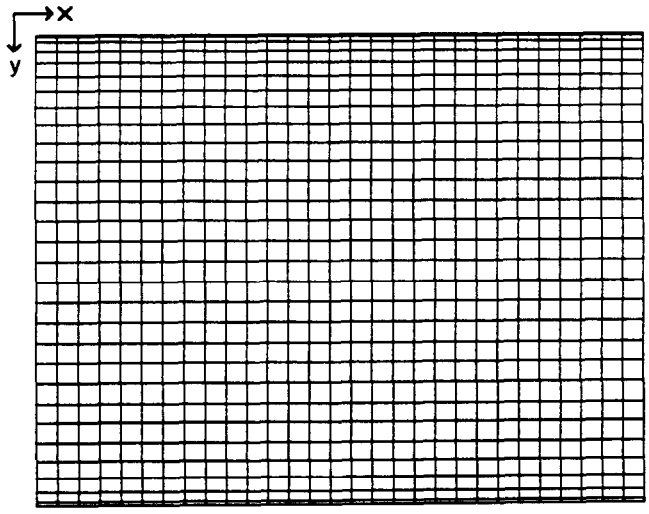

FIG. 2. A typical Fourier–Chebyshev grid in Cartesian coordinates.

To improve stability for the vertical direction we use the coordinate transform described in [3, 2]. A typical mesh is shown in Fig. 2. The Fourier expansions used for the x coordinate are of an odd number length to avoid the indeterminacy of the Nyquist component. The numerical scheme allows for a different number of grid points in the horizontal direction in each of the subdomains. Whenever continuity conditions need to be applied on a boundary adjoining two subdomains, values on the subdomain with the smaller number of points are interpolated to the points of the subdomain with the finer mesh using the Fourier transform itself as the interpolator. After application of the continuity condition, the values are interpolated back to the coarser mesh. These operations can be carried out with use of the fast Fourier transform (FFT).

The boundary conditions are a free surface boundary condition at the top of the mesh $y = 0$ and an absorbing boundary at the bottom $y = L$. In addition, to avoid wraparound and spurious reflections from grid boundaries, an absorbing strip as described in [8] was added on the sides and bottom of the numerical mesh.

The advancement of the solution in time was carried out by a fourth-order Taylor method.

EQUATION OF MOTION IN CIRCULAR COORDINATES

For circular coordinates the equations of motion can be written as a coupled system given by

$$\frac{\partial}{\partial t} \begin{pmatrix} \dot{u}_\theta \\ \dot{u}_r \\ \sigma_{\theta\theta} \\ \sigma_{rr} \\ \sigma_{r\theta} \end{pmatrix} = \mathbf{B} \begin{pmatrix} \dot{u}_\theta \\ \dot{u}_r \\ \sigma_{\theta\theta} \\ \sigma_{rr} \\ \sigma_{r\theta} \end{pmatrix}_r + \frac{1}{r} \mathbf{A} \begin{pmatrix} \dot{u}_\theta \\ \dot{u}_r \\ \sigma_{\theta\theta} \\ \sigma_{rr} \\ \sigma_{r\theta} \end{pmatrix}_\theta + \begin{pmatrix} \frac{2}{\rho r} \sigma_{r\theta} + f_\theta/\rho \\ \frac{1}{\rho r} (\sigma_{rr} - \sigma_{\theta\theta}) + f_r/\rho \\ \frac{\lambda + 2\mu}{r} \dot{u}_r \\ \frac{\lambda}{r} \dot{u}_r \\ -\frac{\mu}{r} \dot{u}_\theta \end{pmatrix}. \tag{11}$$

r and θ respectively denote the radial and angular coordinates, $\dot{u}_r$ and $\dot{u}_\theta$ are the particle velocities in the r and θ directions, and σ_{rr}, $\sigma_{\theta\theta}$, and $\sigma_{r\theta}$ are the stress components. The matrices **A** and **B** are given by (2) and (3).

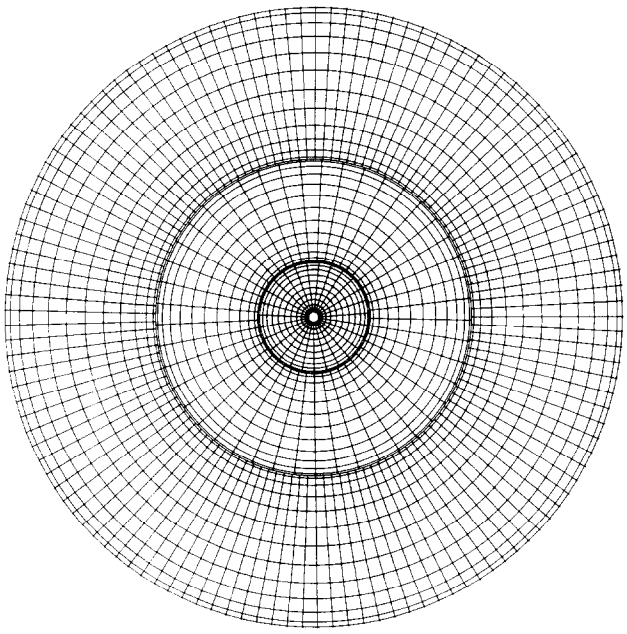

FIG. 3. A typical multi-domain circular grid.

For a fluid region the equations of motion are given by

$$\frac{\partial}{\partial t}\begin{pmatrix}\dot{u}_\theta\\ \dot{u}_r\\ -p\end{pmatrix}=\mathbf{B}\begin{pmatrix}\dot{u}_\theta\\ \dot{u}_r\\ -p\end{pmatrix}_r+\frac{1}{r}\mathbf{A}\begin{pmatrix}\dot{u}_\theta\\ \dot{u}_r\\ -p\end{pmatrix}_\theta+\begin{pmatrix}f_\theta/\rho\\ f_r/\rho\\ \dfrac{K}{r}\dot{u}_r\end{pmatrix}, \tag{12}$$

where **A** and **B** are as in (5) and (6). The characteristic variables for the circular coordinates are the same as for the Cartesian case when y is replaced by r and x is replaced by θ. The interface conditions (7)–(11) will also be the same.

A typical multi-domain circular grid is shown in Fig. 3. For the solution we used a Fourier expansion for the θ coordinate and the Chebyshev expansion in each subdomain for the r coordinate.

EXAMPLES

Two Equal Halfspaces in Juxtaposition

For checking the accuracy of the grid matching procedure a comparison of the numerical results with an analytic solution is performed. The medium is a uniform elastic halfspace with P- and S-wave velocities of 2000 m/s and 1155 m/s, respectively. The medium contains two matched grids (I and II). In Fig. 4 the dashed line indicates the numerical interface which is not a physical interface, since the material parameters do not differ. At the top of the upper grid a free surface boundary condition is implemented. The location of the vertical point force is denoted by S and the receivers by R_1 and R_2.

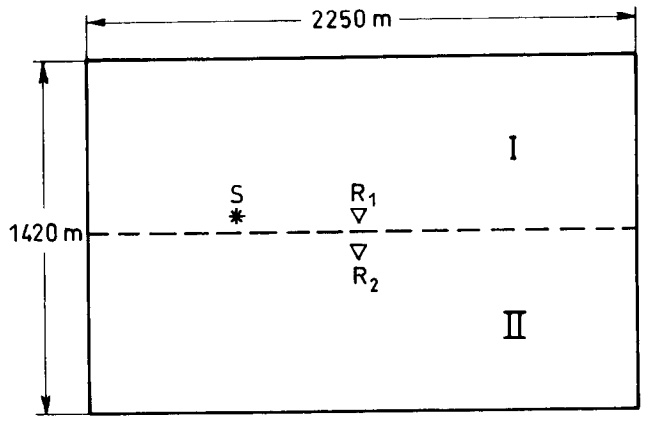

FIG. 4. Source–receiver geometry in a medium set up by two elastic grids.

Figure 5 presents the comparison of numerical results with analytic solutions. The comparison of the vertical and horizontal displacement components at the two receiver positions show very good agreement. Therefore, we conclude that the proposed procedure for matching two elastic grids is accurate and without artificial reflections.

Wave Propagation in a Homogeneous Region in Polar Coordinates

The first test of the solution algorithm in polar coordinates was of wave propagation in a homogeneous region. The problem configuration and the position of the source and the receivers is shown in Fig. 6. The multi-grid consisted of three concentric rings with outer radii of 87 m, 289 m, and 482 m, respectively. The radius of the inner cavity was 5 m. The three rings contained 126 nodepoints in the radial direction while the inner ring contained 45 points in the θ direction, the middle ring contained 125 points in θ, and the outer ring had 225 points. The source was a directional force pointing radially with a Ricker wavelet with a highcut frequency of 50 Hz (i.e., a peak frequency at 25 Hz).

Figure 7 shows amplitude snapshots at respective times $t=0.06$ s, $t=0.12$ s, $t=0.18$ s, $t=0.24$ s, $t=0.3$ s, and $t=0.36$ s. The left-hand panels (Fig. 7a) represent radial particle velocity and the right-hand panels (Fig. 7b) represent motion in the θ direction. These snapshots show two concentric wavefronts of the pressure (P) wave and the shear (S) wave, respectively. It is clear from the figures that the inner cavity, which has a radius smaller than the wavelengths of the pulses propagating in the grid, has very little effect. Figures 8 and 9a and b compare numerically and analytically calculated time histories at the positions shown in Fig. 6. The comparison between the two figures appears very good and no artificial reflections from the subdomain boundaries are apparent.

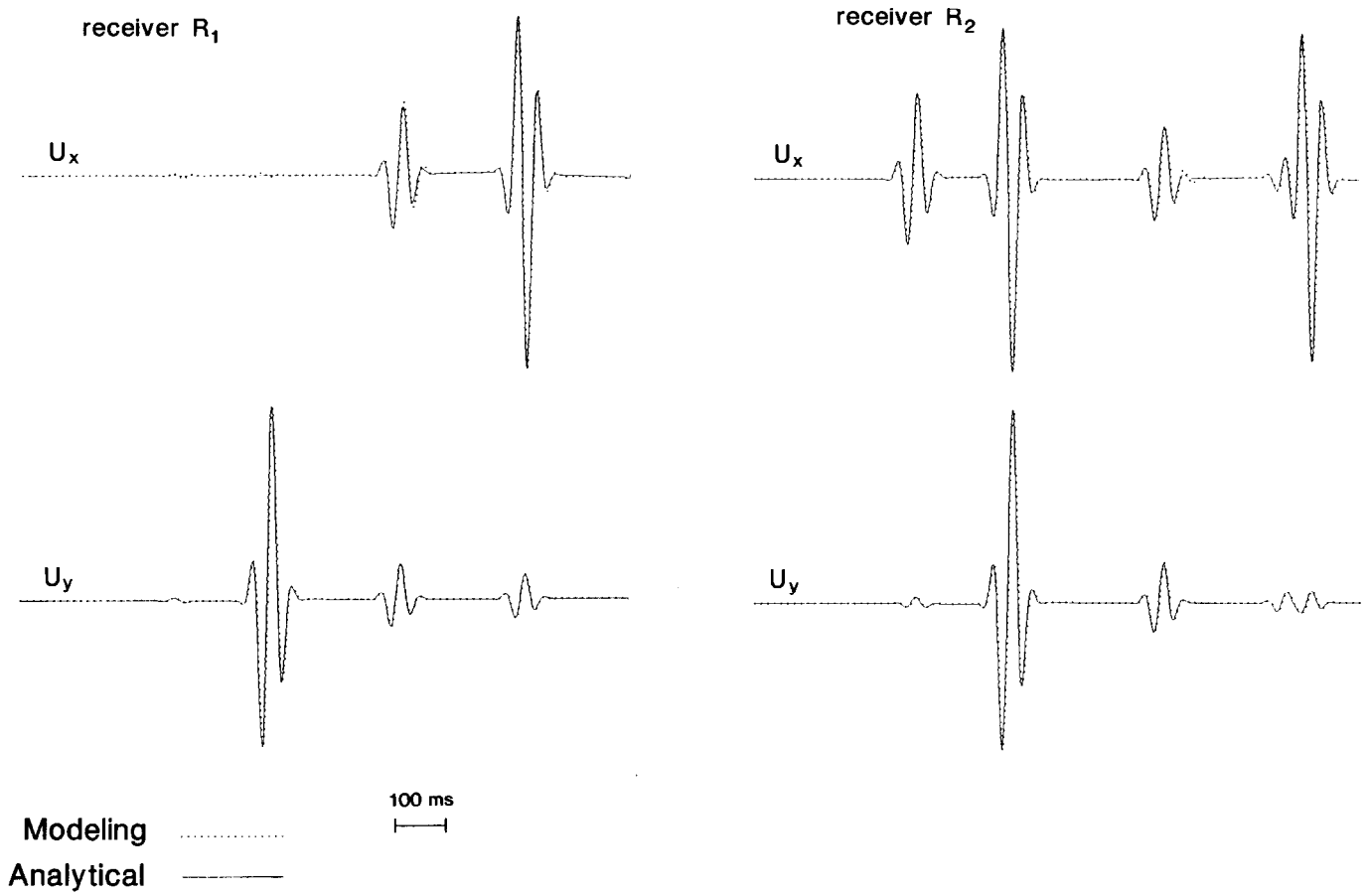

FIG. 5. Comparison of analytical and numerical results at two receiver positions (R_1 and R_2 of Fig. 4) for horizontal and vertical displacements.

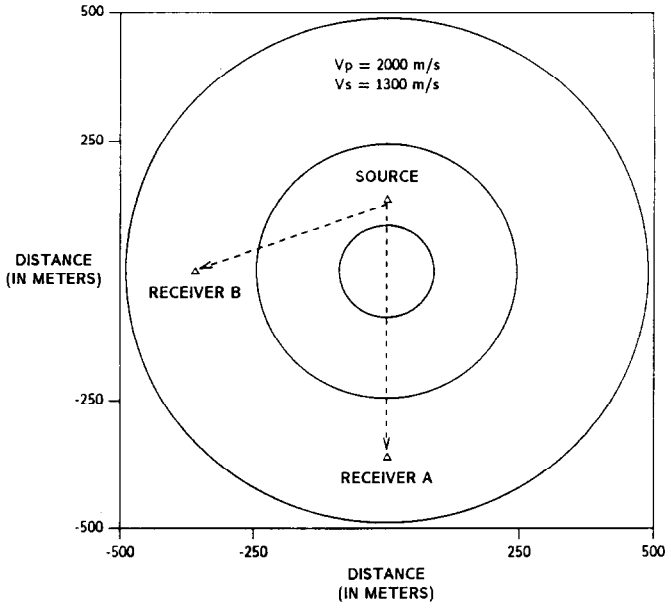

FIG. 6. Source–receiver geometry in a homogeneous medium set up by three concentric grids.

Wave Propagation in a Region Containing Two Halfspaces in Planar Contact

This example examines the solution algorithm for a structure which contains a material discontinuity transversing the boundary between subdomains. The problem configuration is shown in Fig. 10. The calculations used two subdomains with outer radii of 84 m and 322 m, respectively. The radius of the interior cavity was 5 m. Each subdomained contained 126 points in the radial direction. The inner region had 125 points in the angular direction, while the outer region had 225 points.

Figure 11 represents amplitude snapshots at times 0.04 s, 0.80 s, 0.12 s, 0.16 s, 0.20 s, 0.24 s, and 0.28 s, respectively. The figures on the left (Fig. 11a) show the radial particle velocity while the figures on the right (Fig. 11b) represent particle velocities in the θ direction. The figures show well the six separate phases of the incident P and S waves, the P and S waves reflected from the material interface, and the P and S waves transmitted into the lower medium.

Figure 12 shows a comparison between numerical and analytical solutions based on Cagniard's technique (e.g.,

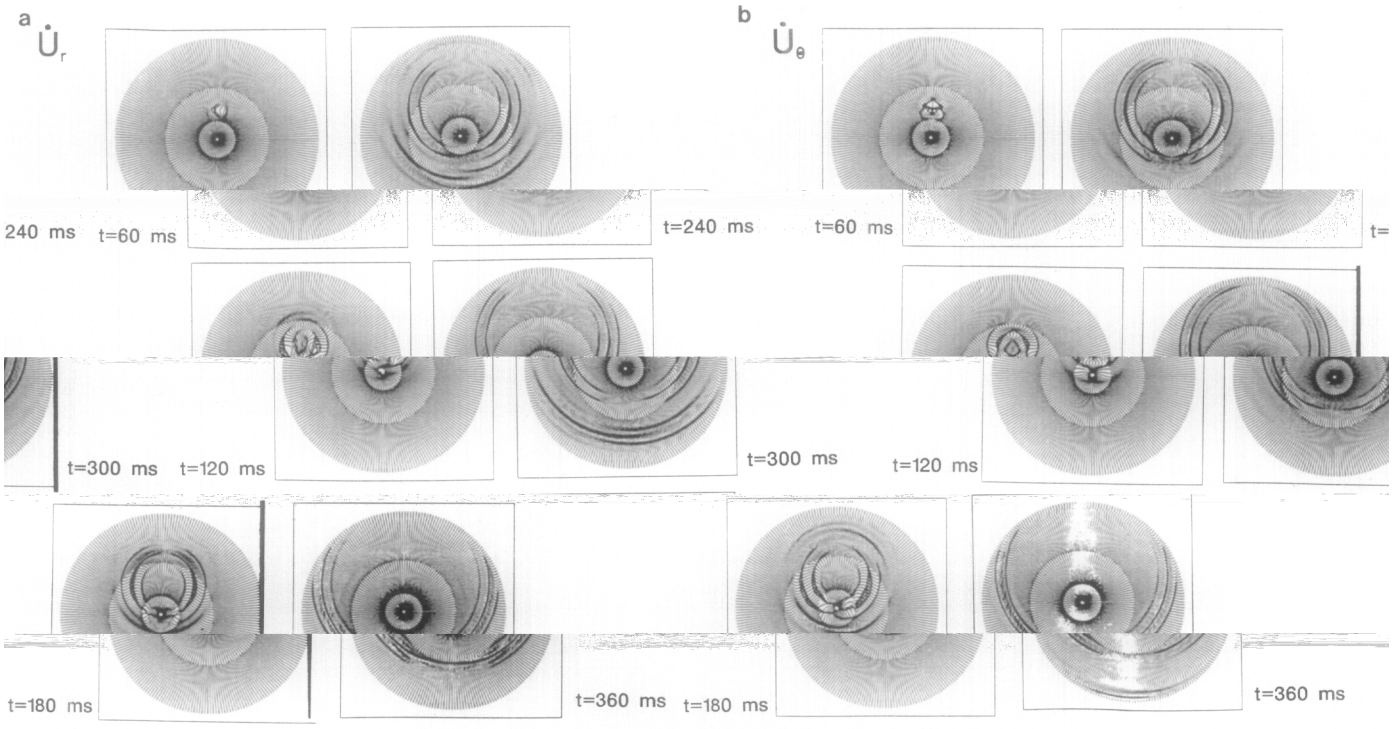

FIG. 7. Snapshots of radial (a) and angular (b) particle velocities at the times given in the figures.

[9]) for the source and receiver positions as shown in Fig. 10. The agreement appears to be very good.

Acoustic Layer over an Elastic Halfspace

In the final example an acoustic layer with a free surface boundary condition of 320 m thickness over an elastic halfspace is modeled. The material parameters in the water

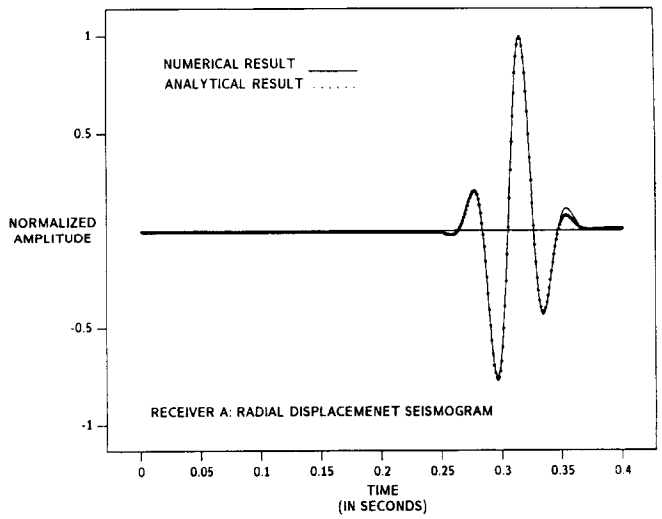

FIG. 8. Comparison of analytical and numerical solution at receiver position A of Fig. 6.

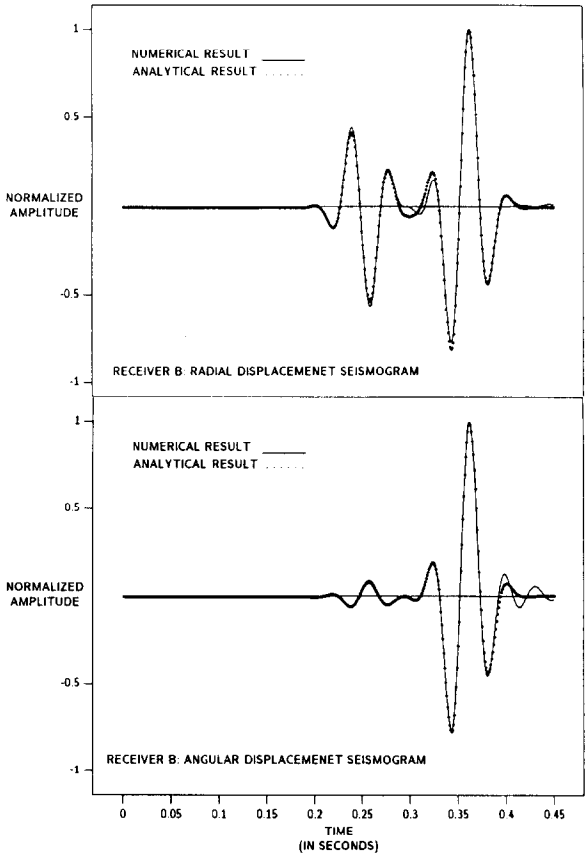

FIG. 9. Comparison of analytical and numerical solutions at receiver position B of Fig. 6: (a) radial; (b) angular displacement.

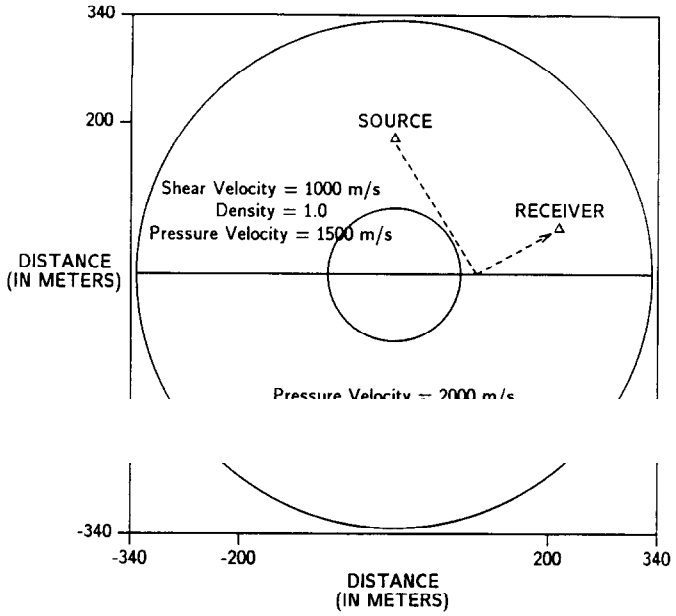

FIG. 10. Source–receiver geometry in an inhomogeneous elastic medium with a planar reflector set up by two concentric grids.

layer are $v_p = 1500$ m/s and, in the elastic halfspace, $v_p = 2000$ m/s and $v_s = 1155$ m/s. The density is constant.

Figure 13 shows the source–receiver geometry. The postions of the pressure source and the receivers were 40 m and 70 m above the interface, respectively. In Fig. 14 a comparison with the analytical solution at the three receivers (R_1, R_2, and R_3) is given. The horizontal distances to the source are 200 m, 600 m, and 1000 m, respectively. The seismograms consist of direct and multiple reflected arrivals as well as a head wave and an interface wave. The agreement with the analytical solution appears very good. Thus also in the acoustic/elastic multi-domain situation the algorithm

CONCLUSION

We have presented a multi-domain Chebyshev–Fourier algorithm for the solution of the equations of dynamic elasticity. We demonstrated the scheme for two-dimensional

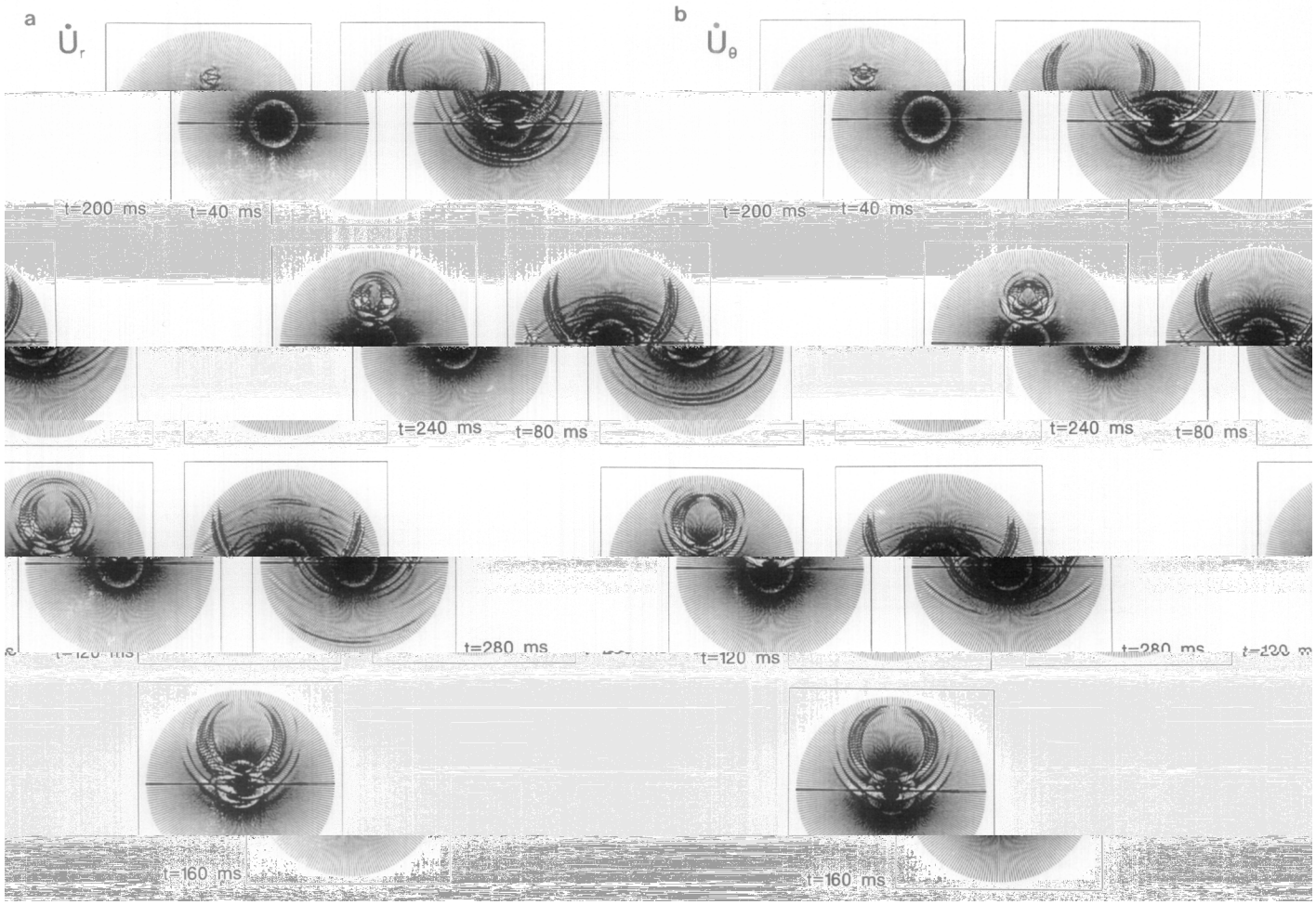

FIG. 11. Snapshots of radial (a) and angular (b) particle velocities at the times given in the figures.

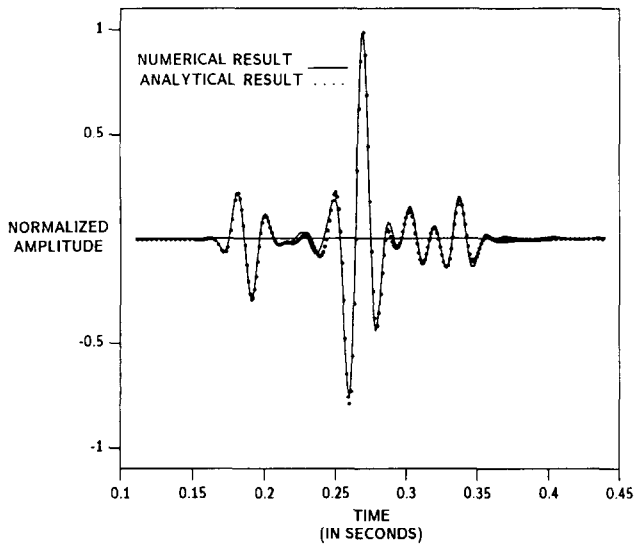

FIG. 12. Comparison of analytical and numerical solution.

problems in Cartesian and polar coordinates. Comparisons between numerical and analytical solutions have shown very good fit with comparable accuracy to solutions with a single domain. No spurious reflections from the boundaries between the subdomains were observed.

The multi-domain approach adds flexibility to global solution techniques such as the Chebyshev–Fourier algorithm used in this study. Of particular importance is the ability to change the grid size. In the context of seismic applications very often the wave velocities near the surface of the earth are much lower than the velocities at depth. Consequently a finer grid near the surface and a coarser grid at depth can effectively allow the use of a larger time step. For polar grids the multi-domain approach may yet be even more beneficial. Use of progressively more grid points in the θ direction with expanding r yields a relatively uniform mesh, hence counteracting the property of polar grids to expand radially.

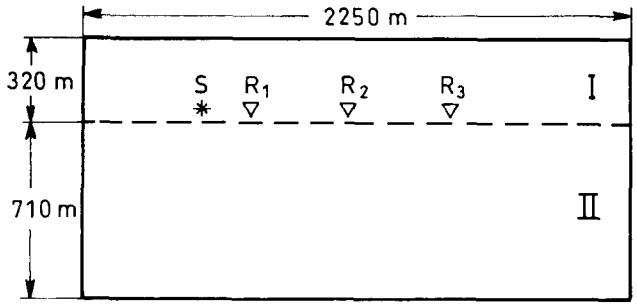

FIG. 13. Source–receiver geometry for the case of an acoustic layer overlaying an elastic halfspace.

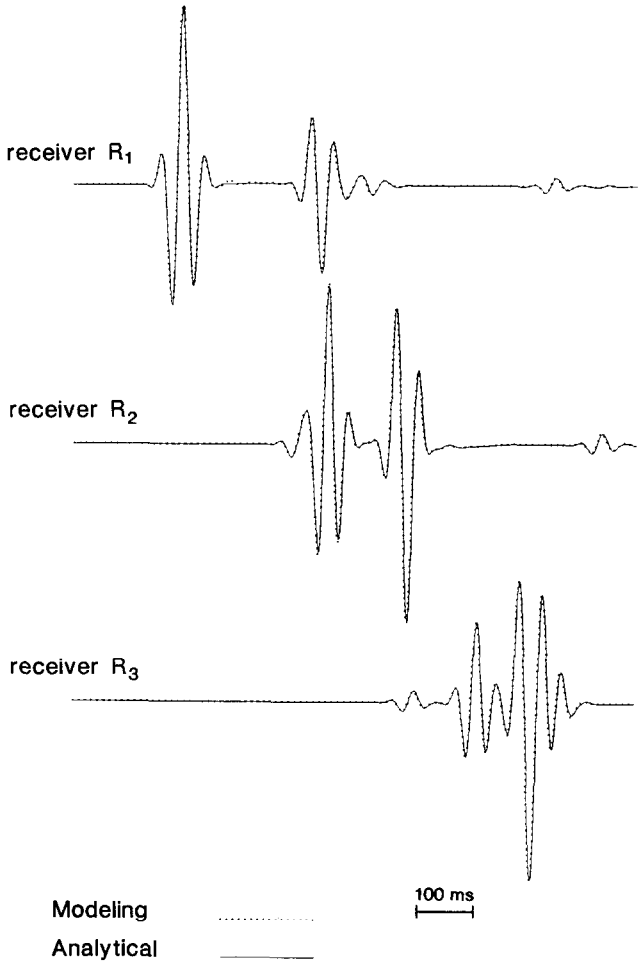

FIG. 14. Comparison of analytical and numerical results (pressure) at three receiver positions (R_1, R_2, and R_3 of Fig. 13).

ACKNOWLEDGMENTS

The authors thank Flemming If and Per Berg, Technical University of Denmark (LAMF), for providing the program for the analytical solution in the acoustic/elastic case. This work was supported by the Commission of the European Communities (JOUF-0033-C(MB)).

REFERENCES

1. C. Canuto, M. Y. Hussaini, A. Quateroni, and T. A. Zang, *Spectral Methods in Fluid Dynamics* (Springer, New York, 1988).
2. D. Kosloff, D. Kessler, A. Q. Filho, E. Tessmer, A. Behle, and R. Strahilevitz, *Geophysics* **55**, 734 (1990).
3. D. Kosloff and H. Tal-Ezer, *J. Comput. Phys.*, submitted.
4. J. Virieux, *Geophysics* **51**, 888 (1986).
5. A. R. Levander, *Geophysics* **53**, 1425 (1988).
6. A. Bayliss, E. K. Jordan, B. J. LeMesurier, and E. Turkel, *Bull. Seis. Soc. Am.* **76**, 1115 (1986).
7. D. Gottlieb, M. Gunzburger, and E. Turkel, *SIAM J. Num. Anal.* **19**, 671 (1982).
8. R. Kosloff and D. Kosloff, *J. Comput. Phys.* **63**, 363 (1986).
9. K. Aki and P. G. Richards, *Quantitative Seismology, Theory and Methods* (Freeman, San Francisco, 1980).